Proceedings of the 21st ICSMGE, Vienna, Austria, 14 – 19 June 2026. Pistrol, Adam & Schweiger (eds.)
Published by: ÖGG, Austrian Society for Geomechanics, Salzburg, Austria, ISBN 978-3-9503898-4-5
https://doi.org/10.53243/ICSMGE2026-968

Effect of secondary reinforcement layers on the performance of GRS walls: a numerical study

Luiz Augusto da Silva Florêncio
Department of Civil Construction, Polytechnic school, Federal University of Rio de Janeiro, Rio de Janeiro, Brazil, luiz.florencio@poli.ufrj.br

Maurício Ehrlich, Seyed Hamed Mirmoradi
Department of Civil Engineering, COPPE, Federal University of Rio de Janeiro, Rio de Janeiro, Brazil.

ABSTRACT: Larger vertical reinforcement spacing (S_V) values in geosynthetic reinforced soil (GRS) walls may lead to global instability, facing detachment, increased connection load and downdrag effects. A practical solution to mitigate these issues is the inclusion of intermediate secondary reinforcement layers, typically 1 m in length. The present study numerically investigates the combined effects of secondary reinforcement length and stiffness, facing-reinforcement connection condition and S_V values, on the performance of GRS walls under working stress conditions. Field data from a well-instrumented full-scale GRS wall were utilized for model validation. The results demonstrate that the inclusion of secondary reinforcement decreases the maximum tensile load in primary reinforcements (T_{max}) and the lateral wall displacement. Moreover, the secondary reinforcement inclusion moves the location of T_{max} from the connection to a distance corresponding to the length of the secondary reinforcement layers. However, the beneficial effects of increasing secondary reinforcement stiffness depend on the secondary reinforcement length, reflecting a combined effect. For a constant relative soil-reinforcement index, different vertical reinforcement spacing values may not affect the distribution of T_{max} values and locations for GRS walls with and without secondary reinforcements.

KEYWORDS: Geosynthetic-reinforced soil walls, numerical modelling, secondary reinforcement, facing-reinforcement connection.

1 INTRODUCTION

The internal ultimate limit states from geosynthetic reinforced soil (GRS) walls include reinforcement rupture, reinforcement pullout, facing detachment, local instability and reinforcement-facing connection failure. The origin of many internal stability problems can be associated with the adoption of large vertical reinforcement spacing (S_V).

The recommended vertical reinforcement spacing for geosynthetic reinforced soil walls with modular block facing should be limited to no more than twice the depth of the facing, measured from the front to the back. Generally, the S_V value should not exceed 0.8 m.

An efficient field compaction operation can be applied to enhance soil performance by increasing its strength and stiffness. In addition, intermediate reinforcements, typically 1.0 m in length, can be included near the facing in order to increase local stability. Since these short reinforcements are not, in principle, designed to mobilize the loads necessary for global stability, they are called secondary reinforcements.

Secondary reinforcements are initially assigned to decrease S_V values without the same executive and cost expense as the primary reinforcements. They can be included in any GRS wall construction system. For example, the reinforcement wrap length in a flexible wrapped-face wall can be understood as a secondary reinforcement condition. In addition to its initial application, several studies showed that the secondary reinforcement can reduce connection and maximum primary reinforcement loads (T_{max}); increase stability near wall facing; reduce displacements; alleviate downdrag forces and change wall failure mode (e.g. Ling et al., 2000; Leshchinsky and Vulova, 2001; Lelli et al., 2015; Gu et al., 2017; Jiang et al., 2016, 2019, 2020).

However, none of the previous studies evaluated the combined effect of secondary reinforcement length and stiffness with other controlling factors of GRS walls, as connection type. Moreover, there is no assessment of the influence of secondary reinforcement on the location of T_{max} for primary reinforcements. T_{max} location is an important indicator of the internal failure surface in GRS walls, required for internal design (Mitchell and Villet, 1987; Juran and Christopher, 1989; Christopher et al., 1990), analytical frameworks methods and failure mode investigations (e.g. Correia et al., 2011; Jacobs et al., 2016; Benmebarek and Djabri, 2017; Abu-Farsakh et al., 2019; Morsy, 2021).

Based on extensive and high-quality instrumented field data of a GRS wall with secondary reinforcement (Jiang et al. 2016), the present study numerically evaluated the effect of secondary reinforcements under working stress conditions, evaluating the wall performance in terms of location and value of T_{max}, facing horizontal displacement and impact of different vertical reinforcement spacing.

2 NUMERICAL MODEL VALIDATION

A two-dimensional plane-strain numerical modelling was performed using the finite-element computer software Plaxis (e.g. Brinkgreve and Vermeer, 2024). The numerical model geometry reproduced the real instrumented GRS wall from Jiang et al. (2016). The model includes a vertical block facing of 11.7 m height, an 18.6 m long reinforced soil, a 17.4 m long retained soil region, a 20 m deep soil foundation, a 2.2 m height embedment soil in front of the wall facing and a 5 m height asymmetric backslope at the wall top. The bottom of the model was fixed in both orthogonal directions and the left and right sides were fixed horizontally but set to be free vertically. Triangular elements with 15 nodes were used in the model, and a fine mesh was used to divide the backfill and retained soil into discrete segments. The model had a total of 14,452 elements and 118,294 nodes. A sensitivity analyses were performed to define the numerical mesh until the performance of the model was not affected by the mesh size and geometric boundary limits.

Input parameters were based on field measurements, the numerical validation of the same GRS wall by Jiang et al. (2019) and from triaxial tests conducted on the reinforced soil fill. The reinforced soil performance was modelled with the Hardening Soil model (HS model), which correlates the soil stiffness with the strain level and the confining stress. The HS model properly captures the soil stiffness under loading-unloading conditions, which is essential to simulate

compaction-induced stress correctly. Four types of 18.3 m primary reinforcements, distributed in two vertical spacings (0.4 and 0.6 m), were modeled with a linear elastic material model, with secant tensile stiffness modulus varying from 360 to 860 kN/m. In addition, there are 1.3 m long secondary reinforcements in every layer between primary reinforcements, with a 330 kN/m stiffness modulus. A model without secondary reinforcements was also modeled with the same characteristics except that it lacks the aforementioned secondary reinforcement.

The numerical model was constructed in stages. In general, the stages sequence include the foundation equilibrium under gravitational conditions, placement and compaction of 0.2 m thick soil layers, inclusion of the reinforcements in their respective wall heights and activation of backslope and embedment soils. The soil compaction was modelled with an 8 kPa induced stress (e.g., Jiang et al. 2019, 2020) with a single loading-unloading cycle of equally distributed load at the top and bottom of each soil layer (e.g., Mirmoradi and Ehrlich, 2014a, 2015, 2018; Scotland et al., 2016; Mirmoradi et al., 2020; Nascimento et al., 2020; Ehrlich et al., 2021; Wang et al., 2022).

To more accurately represent field conditions, the numerical model investigated two type of connections between the facing and the reinforcement: loose and tight. These were based on the field conditions reported by Jiang et al. (2016).

Table 1 gives the input parameters for reinforced soil zone used in this validation procedure. More details about the numerical validation process, wall geometry and input parameters can be found in Florêncio et al. (2025).

Table 1. Input parameters for the reinforced soil zone in validation analysis.

Parameter	Values
Unit weight, γ (kN/m³)	18.1
Cohesion, c (kPa)	1
Soil (plane strain) friction angle, ϕ' (°)	52
Dilation angle, ψ (°)	8
Reference pressure, p_{ref} (kPa)	100
Unloading/reloading Poisson's ratio, υ_{ur}	0.1
Stress dependence exponent, m	0.52
Failure Ratio, R_f	0.9
Coefficient of pressure at rest, K_0	0.248
E_{50}^{ref} (MPa)	31.50
E_{oed}^{ref} (MPa)	29.25
E_{ur}^{ref} (MPa)	109.8

Figure 1 shows the normalised distribution of maximum primary reinforcement load plotted against normalised wall height, with and without secondary reinforcement inclusion and after backslope construction. For the model with secondary reinforcement, two connection conditions were employed. The field measurements represent a wall section with secondary reinforcement (red square symbol) and field instrumentation measurements in a wall section without secondary reinforcement (red triangle symbol). The Rankine active state line is also presented for the internal friction angle used in numerical validation. The shaded area in the graph represents the height of embedment soil in front of the wall facing.

In general, there is a good match between field monitoring data and numerical predictions. The measured and numerically calculated data indicate an increase in T_{max} with depth up to the top of toe embedment; thereafter, it decreases due to toe restraint. Moreover, Figure 1 shows that the inclusion of secondary reinforcement reduces T_{max} to values below the Ka line. Considering a tight connection between block facing and primary reinforcements, the T_{max} values are slightly higher compared to the loose connection condition.

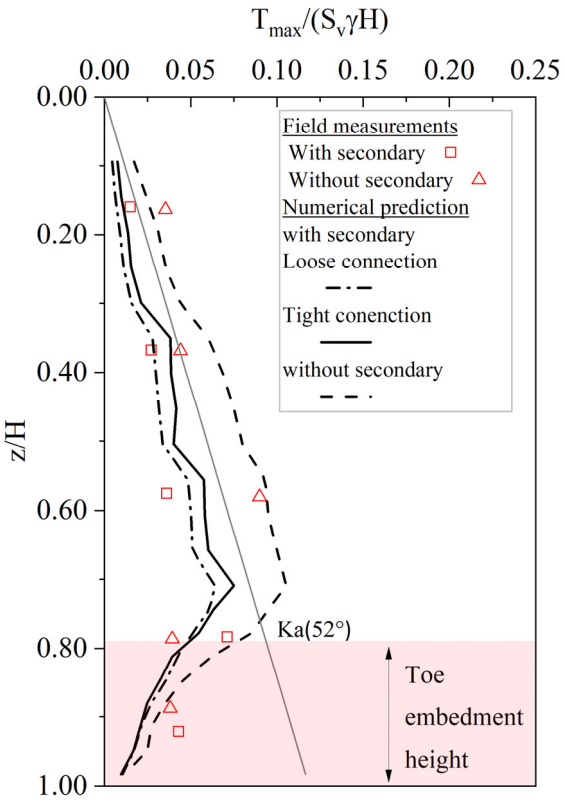

Figure 1. Distribution of normalized maximum tensile stress from field measurements and numerical predictions.

Figure 2 shows the lateral wall displacement at the end of construction [Figure 2a] and after backslope construction [Figure 2b]. The field measurements include wall section with and without secondary reinforcements. The numerical predictions correspond to the field location of the vertical inclinometer, 0.35 m behind the wall facing, considering two conditions for reinforcement connections.

As shown, the numerical models demonstrate good predictive capability compared to the field monitoring data. It is observed that there is a decrease in lateral displacement with secondary reinforcement inclusion. For models with secondary reinforcement, a tight connection between reinforcement and wall facing leads to a decrease in lateral wall movement.

3 PARAMETRIC STUDY

The parametric study was conducted with a modified version of the validation model. The modifications were employed to simplify the model, ensure the expected performance of a GRS block-facing wall and follow the common practice in the design of GRS walls. The modifications include the following: the backslope was removed from the wall top; the embedment soil was removed from the facing toe; the primary reinforcement length was fixed as 0.7 times the wall height; the primary vertical reinforcement spacing was fixed at 0.4 m; all primary reinforcements had the same stiffness (800 kN/m in the baseline model); only tight connector contact between reinforcement and block facing and the value of the backfill soil friction angle

in reinforced zone was changed to 40°, consequently modifying all parameters related to it.

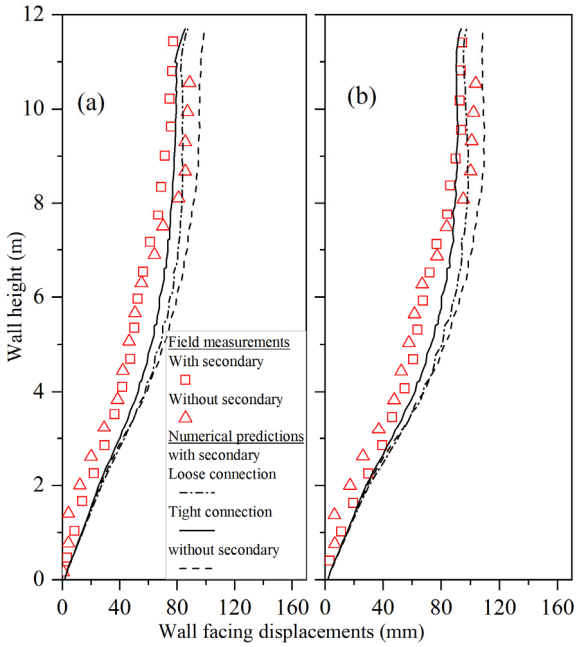

Figure 2. Comparison of lateral wall displacements from field measurements and numerical predictions: (a) end of construction (b) after backslope construction.

For parametric analysis, despite the difference in primary reinforcement spacing and reinforcement stiffness, the value of the relative soil-primary-reinforcement stiffness index, S_{ip}, defined by Ehrlich and Mitchell, 1994, was kept constant. For this study, considering the atmospheric pressure and the modulus number of the hyperbolic stress-strain curve as constants, a simplified form of S_i is:

$$S_i = J_r/S_v \quad (1)$$

From equation (1): J_r is the secant tensile stiffness modulus of reinforcement and S_v is the vertical reinforcement spacing. In parametric study, was used the relation S_{is}/S_{ip}, wich is a index that relates the soil-reinforcement stiffness for each type of reinforcement. S_{is} is the relative soil-reinforcement stiffness index of the secondary reinforcement.

Table 2 presents the conditions of the parametric study. The asterisk determines the baseline model values. For all analyses, the facing was vertical, the wall height was 11.7 m and the S_v between secondary reinforcement was 0.4 m. The secondary reinforcement length is considered from the external face of the block.

Table 2. Conditions of the parametric study.

Parameter	Values/Conditions
Secondary reinforcement	
Length, L_s: m	0.8, 1.3*, 1.8 and 2.3
Stiffness, J_{rs}: kN/m	400, 800*, 1600 and 16000
S_{is}/S_{ip}	0.5, 1.0*, 2.0 and 20
Primary reinforcement	
Stiffness, J_{rp}: kN/m	800*, 1200, 1600 and 2000
Vertical spacing, S_v: m	0.4*, 0.6, 0.8 and 1.0

4 RESULTS AND DISCUSSION

Figure 3 indicates the normalised wall height (h/H), where h is the height from the wall bottom and H is the total wall height, plotted against normalised values and locations of T_{max} in primary reinforcement. The results presented in Figure 3 are related to the baseline model without secondary reinforcement and with different values of S_v. The stiffness of primary reinforcement changed according to the S_v in order to maintain a constant value of S_{ip}. The active state condition (Ka line) is also presented as a reference.

Despite the difference in the S_v, the T_{max} values and location did not change since the S_{ip} is kept constant. Without secondary reinforcement the T_{max} values [Figure 3a] are equal or slightly higher than the Ka line for reinforcement layers approximately above 3.5 m from the GRS wall bottom. Due to the combined effects of the block facing stiffness and toe resistance, the T_{max} values are lower than the corresponding Ka line near the wall bottom. This behavior agrees with several other studies found in literature (e.g., Rowe and Ho, 1993, 1997; Ho and Rowe, 1996; Liu and Won, 2009; Han and Leshchinsky, 2010; Ehrlich and Mirmoradi 2013; Mirmoradi and Ehrlich 2014, 2016, 2017; Mirmoradi et al., 2016, 2021; Jiang et al., 2019). Furthermore, the location of the T_{max} in the primary reinforcement [Figure 3b] was at the connections, except for the reinforcement layers placed near the wall bottom.

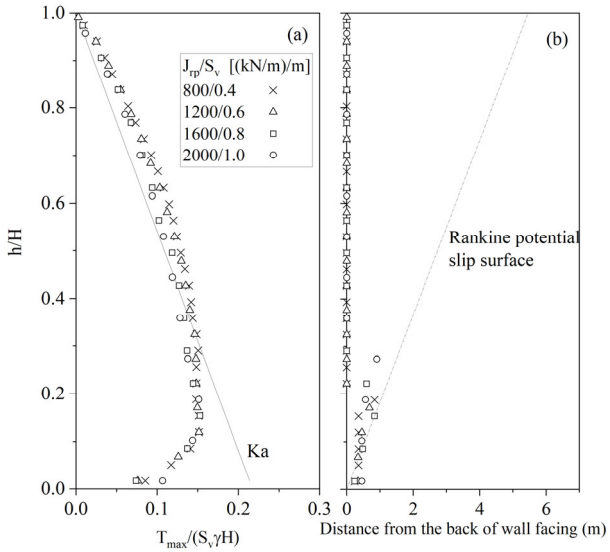

Figure 3. (a) T_{max} values, and (b) T_{max} locations for different vertical spacing values.

Figures 4 and 5 present the effect of secondary reinforcement stiffness and length in the T_{max} value and location, respectively. The shaded area represents the regions of the secondary reinforcement inclusion behind the wall facing. Figure 4 is related to models with the baseline value of L_s and increasing S_{is}/S_{ip}. Figure 5 is related to models with the baseline value of S_{is}/S_{ip} and increasing L_s.

The results from Figure 4a, show that the inclusion of secondary reinforcement reduces the T_{max} in primary reinforcements. Compared to the model without secondary reinforcement, the summation of maximum mobilized loads in primary reinforcement was reduced by about 17% and 27%, for models with S_{is}/S_{ip} of 0.5 and 20, respectively.

Figure 4b indicates that for a constant secondary reinforcement length, higher stiffness shifts the locations of T_{max} from the connection point to a distance equal to the secondary reinforcement length. A stiffer secondary reinforcement is capable to influence a greater number of

primary reinforcement layers in the upper portion of the GRS wall.

Considering the inclusion of secondary reinforcement [Figure 5a], the summation of T_{max} in primary reinforcement decreases approximately 14% and 30% with secondary reinforcement lengths of 0.8 m and 2.3 m, respectively. Due to the increase in L_s, the T_{max} location in primary reinforcements also moves from the block-facing connection to a position corresponding to the secondary reinforcement.

Comparing Figure 4b and Figure 5b, it is evident that the T_{max} location is impacted by the combined effects of the length and stiffness of the secondary reinforcement. A constant S_{is}/S_{ip} has different impact depending on L_s values. The effect of the L_s is more pronounced with higher S_{is}/S_{ip} ratios.

The impact of secondary reinforcement in T_{max} location in the present study is supported by results from Leshchinsky and Vulova (2001), who highlighted that the inclusion of intermediate layers prevents connection failure of the wall. Moreover, the impact of secondary reinforcements is due to the close vertical spacing of the secondary ensemble promoting soil stabilisation near the facing and allowing it to function as an extension of the actual block face. Leshchinsky et al. (1994) and Morsy et al. (2017) also suggested that the secondary reinforcement functions as a monolithic system with its own stiffness.

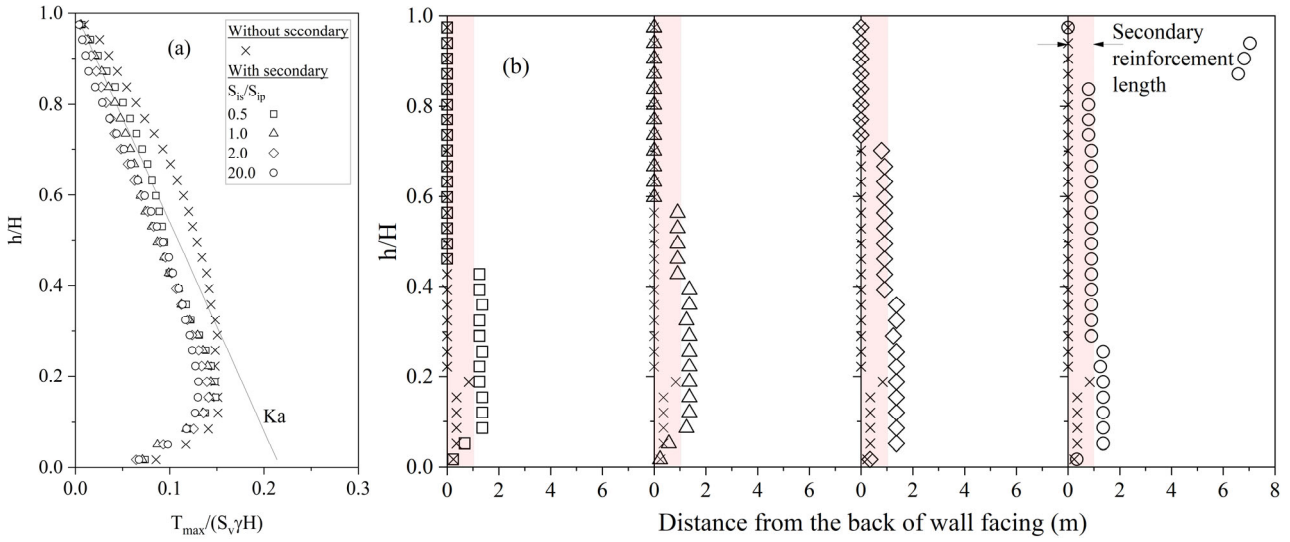

Figure 4. T_{max} (a) values and (b) locations in the primary reinforcement for models with and without secondary reinforcement, S_v = 0,4 m; L_s = 1.3 m and increasing S_{is}/S_{ip}.

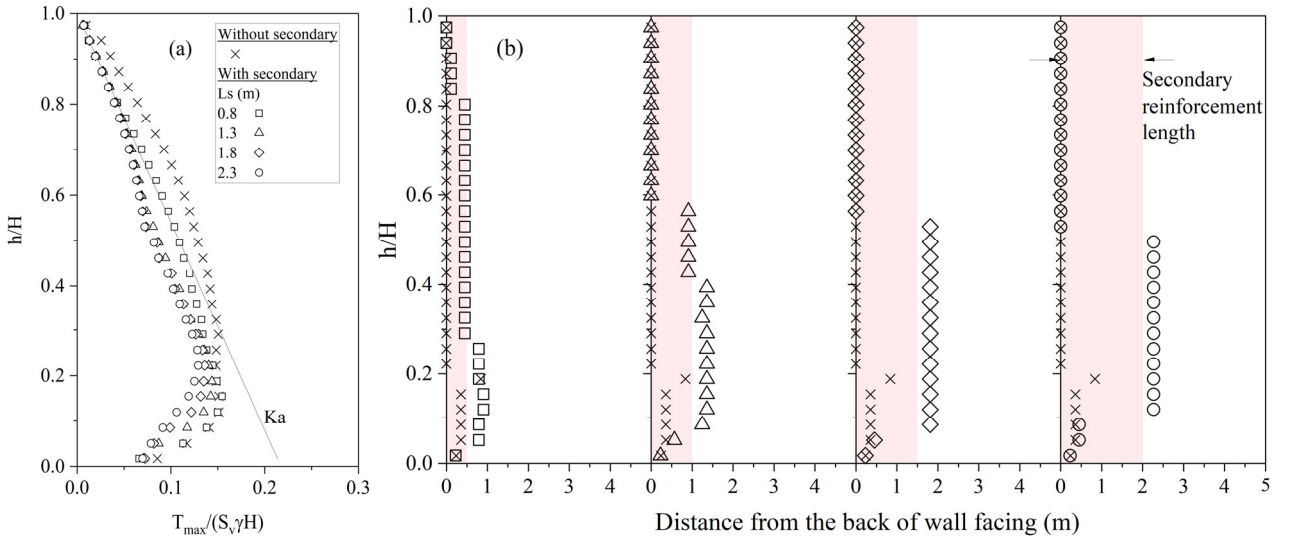

Figure 5. T_{max} (a) values and (b) locations in the primary reinforcement for models with and without secondary reinforcement, S_v = 0,4 m; S_{is}/S_{ip} = 1 and increasing L_s.

Figure 6 illustrates the influence of S_v in the values [Figure 6a] and location [Figure 6b] of T_{max} in primary reinforcements. The numerical results presented in Figure 6 were obtained for models with secondary reinforcement, baseline conditions and S_v equal to 0.4 m and 0.8 m. Of note, for the model with S_v = 0.8 m, the vertical spacing between secondary reinforcements remains equal to 0.4 m, which is the baseline case. Figure 6 shows a similar pattern irrespective of S_v value, demonstrating a consistent behavior of the secondary reinforcements due to the constant S_{is}/S_{ip} ratio. Similar results were obtained from simulation models with other $L_s$values (Florêncio et al. 2025).

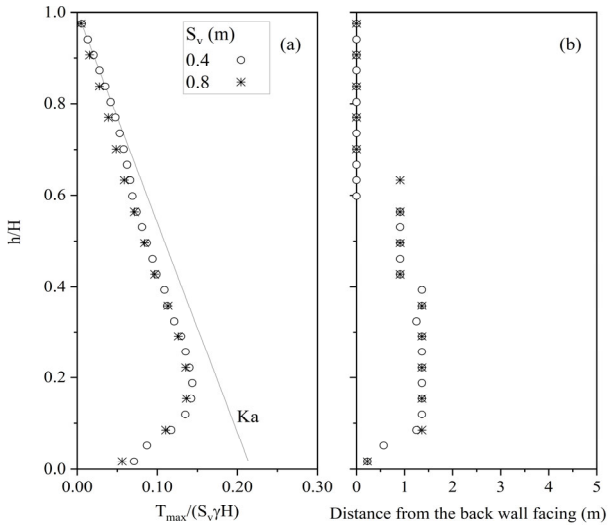

Figure 6. T_{max} (a) values and (b) locations in primary reinforcements for models with secondary reinforcements and different S_v values.

Figure 7 presents the horizontal displacement profile of the wall facing (δ_H) normalized by the total wall height (H) plotted against the normalized wall height (h/H). The numerical facing displacement profile presented in Figure 7 is the horizontal displacement after the correction of facing alignment and inclination carried out after the placement and compaction of each soil layer in the field. For each graph, the secondary reinforcement length is kept constant while the ratio S_{is}/S_{ip} increases. A curve for the numerical model without secondary reinforcement is also presented as a reference.

Compared with the model without secondary reinforcement, the inclusion of secondary reinforcement decreases the horizontal displacements through the combined effect of its length and stiffness. The higher the ratio S_{is}/S_{ip}, the smaller the calculated horizontal displacement. However, the effect of stiff secondary reinforcements is more pronounced for longer L_s. Therefore, in practice, the use of very stiff secondary reinforcement is only beneficial when its length is sufficiently large.

The position of the maximum horizontal displacement remained unchangeed for different L_s. The maximum δ_H occurs about 5.0 m above the wall base and represents less than 1% of the wall height. At the top of the wall, horizontal displacements are close to zero.

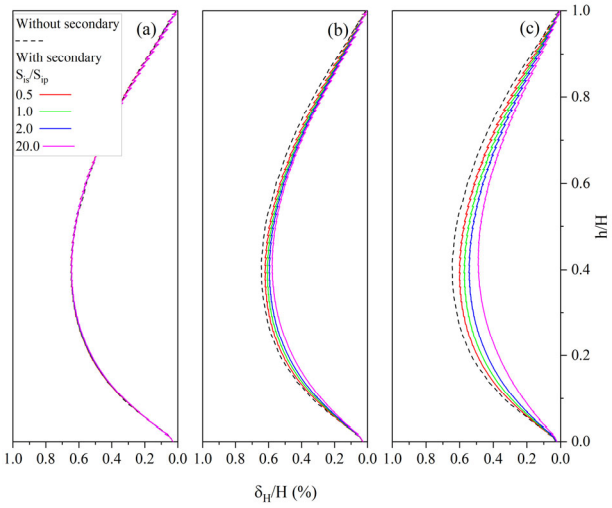

Figure 7. Facing horizontal displacement profiles (a) L_s= 0.8m (b) L_s= 1.3 m (c) L_s= 1.8m.

5 SUMMARY AND CONCLUSIONS

The current research developed a numerical study about the effects of secondary reinforcement inclusion on the value and location of the maximum load along the primary reinforcements and horizontal displacement in GRS walls. The numerical model was validated using Plaxis 2D software based on field monitoring data of a real GRS wall. Parametric analyses were performed to represent typical field conditions. The parametric study aimed to investigate the combined interactions among different factors (e.g., vertical reinforcement spacing, secondary reinforcement length and stiffness and primary reinforcement stiffness). Based on the analyses carried out in the current study, the following conclusions can be drawn:

- A tight connection between block facing and reinforcement reduces facing horizontal displacement and increases the mobilized tensile load in reinforcements.
- For a model without secondary reinforcement, the value and location of maximum tensile load in the primary reinforcement remained unchanged with variations in vertical spacing and reinforcement stiffness when S_{ip} was kept constant.
- A combined effects of secondary reinforcement length and stiffness shift the location of T_{max} in primary reinforcements from the back of the facing to a distance equal to the secondary layer length. Therefore, the facing-reinforcement connection carries a lower load, reducing the possibility of connection failure.
- The secondary reinforcement inclusion reduces the maximum load in the primary reinforcement and horizontal facing displacement through the combined effects of its length and stiffness. The reduction is greater for longer L_s and higher S_{is}/S_{ip} up to certain magnitudes. In general, the effect of the S_{is}/S_{ip} ratio is more evident for longer L_s. This result can be applied in practical design to maximize the performance of the secondary reinforcement.
- A GRS wall with secondary reinforcement exhibits similar behaviour for different S_v values when S_{ip} is constant.
- The region of secondary reinforcement layers behind wall facing may be considered as an 'equivalent facing' because of the stiffer soil response and modified failure mode compared with a GRS wall without secondary reinforcement.

6 ACKNOWLEDGEMENTS

The authors greatly appreciate the funding of this study by the Brazilian Federal Agency for Support and Evaluation of Graduate Education, CAPES, finance code 001, and the National Council for Scientific and Technological Development (CNPq).

7 REFERENCES

Abu-Farsakh MY, Ardah A and Voyiadjis GZ (2019) Numerical parametric study to evaluate the performance of a geosynthetic reinforced soil-integrated bridge system (GRS-IBS) under service loading. *Transportation Geotechnics* 20: 100238, https://doi.org/10.1016/j.trgeo.2019.04.001.

Benmebarek S and Djabri M (2017) FEM to investigate the effect of overlapping-reinforcement on the performance of back-to-back embankment bridge approaches under self-weight. *Transportation Geotechnics* 11: 17–26, https://doi.org/10.1016/j.trgeo.2017.03.002.

Brinkgreve RBJ and Vermeer PA (2024) *PLAXIS: Finite Element Code for Soil and Rock Analyses*. The Manuals of PLAXIS 2024.2 by Bentley Systems, Balkema, Leiden, Netherlands.

Christopher BR, Gill SA, Giroud JP, Juran I, Mitchell, JK, Schlosser F and Dunnicliff J (1990) *Reinforced Soil Structures Volume I. Design and Construction Guidelines*. Federal Highway Administration, McLean, VA, USA, *FHWA-RD-89-043*. https://rosap.ntl.bts.gov/view/dot/972/dot_972_DS1.pdf.

Correia AAS, Pinto MIM and Lopes ML (2011) Design of brick-faced retaining walls reinforced with geotextiles. *Proceedings of the Institution of Civil Engineering – Geotechnical Engineering* 164(5):327–341, https:/doi.org/10.1680/geng.9.00002.

Ehrlich M and Mitchell JK (1994) Working stress design method for reinforced soil walls. *Journal of Geotechnical Engineering* ASCE 120(4): 625–645, https://doi.org/10.1061/(ASCE)0733-9410(1994)120:4(625).

Ehrlich M and Mirmoradi SH (2013) Evaluation of the effects of facing stiffness and toe resistance on the behavior of GRS walls. *Geotextiles and Geomembranes* 40: 28–36. https://doi.org/10.1016/j.geotexmem.2013.07.012

Ehrlich M, Mirmoradi SH and Tortureli M (2021) Numerical evaluation of backfill compaction behind the face of reinforced soil walls. *Proceedings of the Institution of Civil Engineers - Geotechnical Engineering*, 176: 74-85. https://doi.org/10.1680/jgeen.20.00246.

Florêncio LAS, Ehrlich M and Mirmoradi SH (2025) Secondary reinforcement effect on the value and location and maximum reinforcement load. *Proceedings of the Institution of Civil Engineers – Geotechnical Engineering* 178 (1): 15–30, https://doi.org/10.1680/jgeen.23.00048.

Gu M, Collin JG, Han J, Zhang Z, Tanyu BF, Leshchinsky D, Ling HI and Rimoldi P (2017) Numerical analysis of instrumented mechanically stabilized gabion walls with large vertical reinforcement spacing. *Geotextiles and Geomembranes* 45(4): 294–306, https://doi.org/10.1016/j.geotexmem.2017.04.002.

Han J and Leshchinsky D (2010) Analysis of back-to-back mechanically stabilized earth walls. *Geotextiles and Geomembranes* 28(3): 262–267, https://doi.org/10.1016/j.geotexmem.2009.09.012.

Ho SK and Rowe RK (1996) Effect of wall geometry on the behavior of reinforced soil walls. *Geotextiles and Geomembranes* 14(10):521–541, https://doi.org/10.1016/S0266-1144(97)83183-4.

Jacobs F, Ruiken A and Ziegler M (2016) Investigation of kinematic behavior and earth pressure development of geogrid reinforced soil walls. *Transportation Geotechnics* 8: 57–68, https://doi.org/10.1016/j.trgeo.2016.07.004.

Jiang Y, Han J and Parsons RL (2020) Numerical evaluation of secondary reinforcement effect on geosynthetic reinforced retaining walls. *Geotextiles and Geomembranes* 48(1): 98–109, https://doi.org/10.1016/j.geotexmem.2019.103508.

Jiang Y, Han J, Parsons RL and Brennan J (2016) Field instrumentation and evaluation of modular-block MSE walls with secondary geogrid layers. *Journal of Geotechnical and Geoenvironmental Engineering* 142(12): 05016002, https://doi.org/10.1061/(ASCE) GT.1943-5606.0001573.

Jiang Y, Han J, Zornberg JG, Parsons RL, Leshchinsky D and Tanyu B (2019) Numerical analysis of field geosynthetic-reinforced retaining walls with secondary reinforcement. *Géotechnique* 69(2): 122–132, https://doi.org/10.1680/jgeot.17.P.118.

Juran I and Christopher BR (1989) Laboratory model study on geosynthetic reinforced soil retaining walls. *Journal of Geotechnical Engineering* 115(7): 905–926, https://doi.org/10.1061/(ASCE)0733-9410(1989)115:7(905).

Lelli M, Laneri R and Rimoldi P (2015) Innovative reinforced soil structures for high walls and slopes combining polymeric and metallic reinforcements. *Procedia Engineering* 125: 397–405, https://doi.org/10.1016/j.proeng.2015.11.099.

Leshchinsky D and Vulova C (2001) Numerical investigation of the effects of geosynthetic spacing on failure mechanisms in MSE block walls. *Geosynthetics International* 8(4): 343–365, https://doi.org/10.1680/gein.8.0199.

Leshchinsky D, Kaliakin V, Bose P and Collin J (1994) Failure mechanism in geogrid-reinforced segmental walls: experimental implications. *Soils and Foundations* 34(4): 33–41, https://doi.org/10.3208/sandf1972.34.4_33.

Ling HI, Cardany CP, Sun LX and Hashimoto H (2000) Finite element study of a geosynthetic-reinforced soil retaining wall with concrete block facing. Technical paper. *Geosynthetics International* 7(3):163–188, https://doi.org/10.1680/gein.7.0170.

Liu H and Won MS (2009) Long-term reinforcement load of geosynthetic-reinforced soil retaining walls. *Journal of Geotechnical and Geoenvironmental Engineering* 135(7): 875–889, https://doi.org/10.1061/(ASCE)GT.1943-5606.0000052.

Mirmoradi SH and Ehrlich M (2014a) Modeling of the compaction-induced stresses in numerical analyses of GRS walls. *International Journal of Computational Methods* 11: 1342002. *https://doi.org/10.1142/S0219876213420024*

Mirmoradi SH and Ehrlich M (2014b) Numerical evaluation of the behavior of GRS walls with segmental block facing under working stress conditions. *Journal of Geotechnical and Geoenvironmental Engineering* 141(3): 04014109, https://doi.org/10.1061/(ASCE)GT.1943-5606.0001235.

Mirmoradi SH and Ehrlich M (2015) Modeling of compaction-induced stress on reinforced soil walls. *Geotextiles and Geomembranes* 43(1): 82–88, https://doi.org/10.1016/j.geotexmem.2014.11.001.

Mirmoradi SH and Ehrlich M (2016) Evaluation of the effect of toe restraint on GRS walls. *Transportation Geotechnics* 8: 35–44. https://doi.org/10.1016/j.trgeo.2016.03.002

Mirmoradi SH and Ehrlich M (2017) Effects of facing, reinforcement stiffness, toe resistance, and height on reinforced walls. *Geotextiles and Geomembranes* 45(1): 67–76, https://doi.org/10.1016/j.geotexmem.2016.07.006.2017.

Mirmoradi SH and Ehrlich M (2018) Numerical simulation of compaction-induced stress for the analysis of RS walls under working conditions. *Geotextiles and Geomembranes* 46(3): 354–365, https://doi.org/10.1016/j.geotexmem.2018.01.006.

Mirmoradi SH, Ehrlich M and Dieguez C (2016) Evaluation of the combined effect of toe resistance and facing inclination on the behavior of GRS walls. *Geotextiles and Geomembranes* 44(3): 287–294. https://doi.org/10.1016/j.geotexmem.2015.12.003

Mirmoradi SH, Ehrlich M and Magalhães LFO (2021) Numerical evaluation of the effect of foundation on the behavior of reinforced soil walls. *Geotextiles and Geomembranes* 49(3): 619–628. https://doi.org/10.1016/j.geotexmem.2020.11.007

Mirmoradi SH, Ehrlich M and Nascimento G (2020) Experimental, numerical, and analytical investigation of the effect of compaction-induced stress on the behavior of reinforced soil walls. *Soils and Rocks* 43: 419–439. 10.28927/SR.433419

Mitchell JK and Villet WCB (1987) *Reinforcement of Earth Slopes and Embankments*. Transportation Research Board, Washington, DC, USA, NCHRP Report 290.

Morsy AM (2021) Analytical framework for prediction of facing connection loads in reinforced soil walls considering reinforcement downdrag. *Transportation Geotechnics* 30: 100537, https://doi.org/10.1016/j.trgeo.2021.100537.

Morsy AM, Leshchinsky D and Zornberg JG (2017) Effect of reinforcement spacing on the behavior of geosynthetic reinforced soil. In *Geotechnical Frontiers 2017: Walls and Slopes* (Brandon TL and Valentine RJ (eds). American Society of Civil Engineers, Reston, VA, USA, Goetechnical Special Publication 278, pp. 112–125, https://doi.org/10.1061/9780784480458.012.

Nascimento G, Ehrlich M and Mirmoradi SH (2020) Numerical simulation of compaction-induced stress for the analysis of RS walls under surcharge loading. *Geotextiles and Geomembranes* 48(4): 532–538, https://doi.org/10.1016/j.geotexmem.2020.02.011.

Rowe RK and Ho SK (1993) Keynote lecture: a review of the behavior of reinforced soil walls. *In Earth Reinforcement Practice: Proceedings of International Symposium*, Fukuoka, Japan (Ochiai H, Hayashi S and Otani J (eds)). Balkema, Rotterdam, the Netherlands, vol. 2,pp. 801–830.

Rowe RK and Ho SK (1997) Continuous panel reinforced soil walls on rigid foundations. *Journal of Geotechnical and Geoenvironmental Engineering* 123(10): 912–920, https://doi.org/10.1061/(ASCE)1090-0241(1997)123:10(912).

Scotland I, Dixon N, Frost M, Fowmes G and Horgan G (2016) Modelling deformation during the construction of wrapped geogrid-reinforced structures. *Geosynthetics International* 23(3):219–232, https://doi.org/10.1680/jgein.15.00049.

Wang C, Wang L and Liu H (2022) Analyzing the influence of facing batter on reinforcement loads of reinforced soil walls under working stress conditions. *Geotextiles and Geomembranes* 50(6): 1244–1251, https://doi.org/10.1016/j.geotexmem.2022.09.004.